Chinese Journal of Geophysics

Volume 31, Number 3

P-SV Wave Responses for a Point Source in Two-Dimensional Heterogeneous Media: Finite-Difference Approximation

Xie Xiao-bi and Yao Zhen-xing

(Institute of Geophysics, Academia Sinica, Beijing)

A method for producing approximate point source *P-SV* wave responses in laterally varying model is introduced. The method is based on the first-order system of wave equations for the velocities and stresses. First, we introduce the linearly distributed stress tensor as the source, and use a two- dimensional finite-difference scheme to produce the response of this source. Then the point source response is generated by correcting both the waveform and geometrical spreading of the line source response. The accuracy of this approximation is justified by comparing the numerical results with the more accurate solutions. Because any of the dislocation source, explosive source or concentrated body force may be simulated by the sources mentioned above, also, because the finite-difference method has the advantage that arbitrary velocity and density structure in the media may be specified, the method seems to be effective for the problems such as the near source strong ground motions, explosive vibrations and exploration seismology.

Key words: Waves in laterally varying media, Finite-difference method, Synthetic seismograms, Dislocation source.

I. INTRODUCTION

Synthetic seismogram is an effective method for investigating the near source strong ground motions and seismic source processes. In recent years a number of efficient computational methods have been developed for this purpose, of which those widely used are based on the models of horizontally layered medium, such as the discrete wavenumber method (Bouchon, 1979), discrete wavenumber-finite element (DWFE) method (Olson, 1984), generalized ray theory (Helmberger, 1968), generalized reflection-transmission coefficient matrix method (Yao and Harkrider, 1983), Haskell matrix method (Li, 1985). The common advantages of these methods are their highly computational speed and accuracy. But the application of the above methods will be restricted if complicated interfaces or lateral heterogeneities are presented. Under such conditions, the methods based on the discretization of the elastic dynamic equation, such as the finite difference or finite element method, are more effective and have been developed rapidly (e.g., Alterman and Karal, 1968; Kelley et al., 1976; Virieux, 1984, 1986; Bayliss et al., 1986). Most authors adopted two dimensional grids and isotropic linear sources in their finite-difference codes. Such models are not suitable for simulating the sources of natural earthquakes. Although three dimensional media can be modelled theoretically, in practice their applicability is limited by the storage and speed of the present computers. So we intend to develop an approximate method, which can yield the point source response using a two dimensional finite-difference scheme. For the same purpose, Vidale et al (1985), Vidale (1987) developed a method by which the linear source response can be transformed into the point source response. The main deficiency of this method is that there are considerable errors for waves near vertically radiated from the source. Based on the axisymmetric assumption, which was originally introduced by Alterman et al. (1968), Yuan et al. (1986) developed another finite-difference method to deal with the responses of point dislocation sources. Theoretically this is an accurate method, but in most situations the axisymmetric assumption does not suit the real media. In the present research, a method for producing approximate point source P-SV wave responses in laterally varying model is introduced. The method is based on the first-order system of wave equations for velocities and stresses. First, we adopt a linearly distributed stress tensor as the source, and use a two-dimensional finite-difference scheme to produce the response to this source. Then the point source response is generated by correcting both the waveforms and geometrical spreading of the line-source response. The accuracy of this approximation is justified by comparing the numerical results with the more accurate solutions. Because any of the dislocation source, explosion source, and concentrated body force may be simulated by the source mentioned above, also, because the finite-difference method has the advantage that arbitrary velocity and density structure in the media may be specified, the method seems to be effective for calculating synthetic seismograms in a variety of problems of earthquake and exploration seismology.

II. BASIC EQUATIONS AND REPRESENTATIONS OF THE SOURCES

In three dimensional space, the elastic dynamic equation can be written as

$$\rho \dot{u}_i = \frac{\partial}{\partial x_j} \tau_{ji} + s_i, \tag{1}$$

in which u_i is the particle velocity, ρ, the density, τ_{ji}, the stress tensor and s_i the body force density. For a complicated source, s_i is generally not a simple force but a force system. For example, for dislocation source we need a double-couple and three equal and mutually perpendicular linear dipoles are needed for an explosive source. If the concept of generalized function is adopted, the couple and vector dipole without moment can be represented as

$$s_i = -M_{ji} \frac{\partial}{\partial x_j} \delta(x - x_s), \tag{2}$$

in which M_{ji} is the moment tensor, $\delta(x-x_s) = \delta(x_1 - x_{s1})\, \delta(x_2 - x_{s2})\, \delta(x_3 - x_{s3})$ is the three dimensional Dirac function and x_s is the coordinate of the source. Supposing that the velocity field in (1) is zero, the contributions from the traction and the body force should be equal in magnitude but opposite in direction, so we obtain the stress equivalence of the body force source, i.e. equation (2), as

$$\tau_{ji} = -M_{ji} \delta(x - x_s). \tag{3}$$

This means that a force system like equation (2) acted in the media is equivalent to a traction distribution like (3) acted on the same position. In other words, the action of a stress distributed as a Dirac function is equivalent to that of a couple or a vector-dipole without moment. Considering that a body force is equivalent to a discontinuity of the traction, it is easily understood that a couple can be simulated by a Dirac-function-like traction, which has two discontinuities. In a finite-difference code, to give a body force system like equation (2) on one grid point will be very difficult; for this reason, the stress expression (3) will be very useful.

In two-dimensional problems, all the variables will be constant along the x_2 direction, so the SH wave polarized in x_2 direction will be decoupled with the P-SV waves polarized in the x_1ox_3 plane. For P-SV waves the dynamic equation can be written as a first order system

$$\frac{\partial \boldsymbol{w}}{\partial t} = \mathbf{A} \frac{\partial \boldsymbol{w}}{\partial x_1} + \mathbf{B} \frac{\partial \boldsymbol{w}}{\partial x_3} + \boldsymbol{s}_{P\text{-}SV}, \tag{4}$$

where $\mathbf{w} = (u_1, u_3, \tau_{11}, \tau_{33}, \tau_{13})^T$ is a vector composed of the particle velocities and stresses, hence called velocity-stress vector, u_1 and u_3 are the x_1 and x_3 components of the velocity, A and B are coefficient matrices composed of the medium parameters,

$$\mathbf{A} = \begin{bmatrix} 0 & 0 & \rho^{-1} & 0 & 0 \\ 0 & 0 & 0 & 0 & \rho^{-1} \\ \rho\alpha^2 & 0 & 0 & 0 & 0 \\ \rho\beta^2 & 0 & 0 & 0 & 0 \\ 0 & \rho\beta^2 & 0 & 0 & 0 \end{bmatrix}, \quad \mathbf{B} = \begin{bmatrix} 0 & 0 & 0 & 0 & \rho^{-1} \\ 0 & 0 & 0 & \rho^{-1} & 0 \\ 0 & \rho\beta^2 & 0 & 0 & 0 \\ 0 & \rho\alpha^2 & 0 & 0 & 0 \\ \rho\beta^2 & 0 & 0 & 0 & 0 \end{bmatrix}. \tag{5}$$

where α and β are the velocities of the compressional and transverse waves, respectively. The inhomogeneous term

$$s_{P-SV} = (s_1/\rho, s_3/\rho, s_{11}, s_{33}, s_{13})^T \tag{6}$$

is a vector composed of the source functions of *P-SV* wave. All the source functions are linear sources distributed along the x_2 direction, where

$$s_i = F_i\delta(x_1 - x_{r1})\delta(x_3 - x_{r3}) \tag{7}$$

is the body force density, F_i is the linear density of the body force distributed along the x_2 direction.

$$s_{ji} = -m_{ji}\delta(x_1 - x_{r1})\delta(x_3 - x_{r3}) \tag{8}$$

is the traction acting in the media, m_{ji} is the linear density of the moment tensor distributed along the x_2 direction. Note that here the dimension of s_{ji} is still that of stress. In equation (6) there are only three traction components. This means that there are three independent moment tensor components which contribute to the P-SV wave response. $\mathbf{m}$ can be expressed as

$$\mathbf{m} = m_0 s(t) \sum_{i=1}^{3} A_i \mathbf{M}_i, \tag{9}$$

where

$$\left.\begin{aligned} A_1 &= -\cos\delta\cos\lambda\cos\phi + \cos 2\delta \sin\lambda \sin\phi, \\ A_2 &= \sin\delta\cos\lambda\sin 2\phi + \sin 2\delta \sin\lambda\cos^2\phi, \\ A_3 &= \sin 2\delta \sin\lambda. \end{aligned}\right\} \tag{10}$$

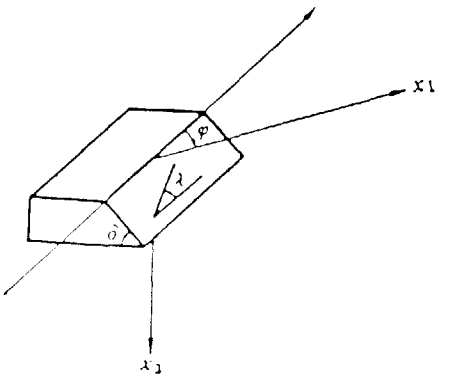

Fig. 1.
Geometry of the fault and receiver

δ and λ are the dip and rake angles of the fault, respectively, ϕ is the angle measured from the strike to the direction of the receiver. The geometry of the fault and receiver is shown in Figure 1.

$$\mathbf{M}_1 = \begin{bmatrix} 0 & 0 & 1 \\ 0 & 0 & 0 \\ 1 & 0 & 0 \end{bmatrix}, \quad \mathbf{M}_2 = \begin{bmatrix} 1 & 0 & 0 \\ 0 & -1 & 0 \\ 0 & 0 & 0 \end{bmatrix}, \quad \mathbf{M}_3 = \begin{bmatrix} -1 & 0 & 0 \\ 0 & 0 & 0 \\ 0 & 0 & 1 \end{bmatrix}. \tag{11}$$

where the quantities with subscripts 1, 2 and 3 correspond with the dip-slip, strike-slip and 45° dip-slip faults, respectively. The contribution from a fault with arbitrary orientation can be easily obtained by summing up the responses of three fundamental faults. m_0 is the linear density of the scalar seismic moment, s(t) is the unit source time history. For an explosive source

$$\mathbf{m} = m_0 s(t)\mathbf{M}, \tag{12}$$

where

$$\mathbf{M} = \begin{bmatrix} 1 & 0 & 0 \\ 0 & 0 & 0 \\ 0 & 0 & 1 \end{bmatrix}.$$

If a concentrated force is to be introduced into the computation, appropriate values should be assigned to s_1 and s_3 in equation (6). Inserting equations (9) to (12) into equation (6) and (4), we can obtain the responses for various linear sources.

III. THE CORRECTIONS FROM THE LINEAR SOURCE TO POINT SOURCE

We intend to obtain the approximate point source responses by computing the linear source responses. There are some differences in the characteristics of waves radiated from these two types of sources. Firstly, the wave from a line source has a long tail in comparison to the clear-cut waveform from a point source. Secondly, the powers of attenuation with distance due to geometrical spreading are different. To approximate the point- source response with the line-source response corrections for both the waveform and the geometrical spreading are needed. For this purpose, we first integrate the point source responses in homogeneous space to obtain the linear source response and make a comparison between these two responses, and then discuss the corrections according to their differences.

Assuming a step-like source time history, the velocity response for a point dislocation source can be obtained from Aki and Richards (1980)

$$\begin{aligned} u_i^P = {} & \frac{1}{4\pi\rho}\left(\frac{15\gamma_i\gamma_j\gamma_k - 3\gamma_i\delta_{jk} - 3\gamma_j\delta_{ik} - 3\gamma_k\delta_{ij}}{R^4}\right) t[H(t - R/\alpha) - H(t - R/\beta)]M_{jk} \\ & + \frac{1}{4\pi\rho\alpha^2}\left(\frac{6\gamma_i\gamma_j\gamma_k - \gamma_i\delta_{jk} - \gamma_j\delta_{ik} - \gamma_k\delta_{ij}}{R^2}\right)\delta(t - R/\alpha)M_{jk} \\ & - \frac{1}{4\pi\rho\beta^2}\left(\frac{6\gamma_i\gamma_j\gamma_k - \gamma_i\delta_{jk} - \gamma_j\delta_{ik} - 2\gamma_k\delta_{ij}}{R^2}\right)\delta(t - R/\beta)M_{jk} \end{aligned} \tag{13}$$

$$+\frac{1}{4\pi\rho\alpha^3}\gamma_i\gamma_j\gamma_k\frac{1}{R}\frac{\partial}{\partial t}\delta(t-R/\alpha)M_{jk}$$
$$-\frac{1}{4\pi\rho\beta^3}(\gamma_i\gamma_j-\delta_{ij})\gamma_k\frac{1}{R}\frac{\partial}{\partial t}\delta(t-R/\beta)M_{jk}. \tag{13}$$

where u_i^P is the x_i component of the velocity field from a point source, $\gamma = R/R$, $R = [(x_1 - x_{s1})^2 + (x_2 - x_{s2})^2 + (x_3 - x_{s3})^2]^{1/2}$ is the source-receiver distance in three dimensions. On the right-hand side of equation (13), the first term is the near-field term, the second and third are the intermediate-field terms , and the fourth and fifth are the far-field terms. Integrating equation (13) along the x_2 direction from $-\infty$ to $+\infty$, the linear source response can be obtained as

$$u_i^L = \frac{1}{2\pi\rho}\left(\frac{8\gamma_i\gamma_j\gamma_k - 2\gamma_i\delta_{jk} - 2\gamma_j\delta_{ik} - 2\gamma_k\delta_{ij}}{r^{3/2}}\right)$$
$$\times(\sqrt{2/\alpha}\sqrt{t-r/\alpha}-\sqrt{2/\beta}\sqrt{t-r/\beta})m_{jk}$$
$$+\frac{1}{2\pi\rho\alpha^2}\left(\frac{4\gamma_i\gamma_j\gamma_k-\gamma_i\delta_{jk}-\gamma_j\delta_{ik}-\gamma_k\delta_{ij}}{r^{3/2}}\right)\sqrt{\alpha/2}\frac{1}{\sqrt{t-r/\alpha}}m_{jk}$$
$$-\frac{1}{2\pi\rho\beta^2}\left(\frac{4\gamma_i\gamma_j\gamma_k-\gamma_i\delta_{jk}-\gamma_j\delta_{ik}-2\gamma_k\delta_{ij}}{r^{3/2}}\right)\sqrt{\beta/2}\frac{1}{\sqrt{t-r/\beta}}m_{jk}$$
$$+\frac{1}{2\pi\rho\alpha^3}\gamma_i\gamma_j\gamma_k\frac{1}{r^{1/2}}\sqrt{\alpha/2}\frac{\partial}{\partial t}\left(\frac{1}{\sqrt{t-r/\alpha}}\right)m_{jk}$$
$$-\frac{1}{2\pi\rho\beta^3}(\gamma_i\gamma_j-\delta_{ij})\gamma_k\frac{1}{r^{1/2}}\sqrt{\beta/2}\frac{\partial}{\partial t}\left(\frac{1}{\sqrt{t-r/\beta}}\right)m_{jk}, \tag{14}$$

where $\gamma = r/r$, $r = [(x_1 - x_{s1})^2 + (x_3 - x_{s3})^2]^{1/2}$ is the source-receiver distance in two dimensions. In equation (14) the approximation t—r/c (c is α or β) has been introduced. For convenience, we set the point source at the origin; set the linear source along the x_2 axis, and discuss the problem in x_1ox_3 plane, in this case $r = R$. For *P-SV* wave response i, j, k≠2. A comparison between equations (13) and (14) shows that the most obvious differences come from the pulse shapes and geometrical spreading factors. Table 1 lists the main differences.

Table 1

The main differences between the responses for both point and linear sources

	waveform		geometric spreading	
	point source	linear source	point source	linear source
near field	$H(t-R/\alpha)-H(t-R/\beta)$	$\sqrt{t-r/\alpha}-\sqrt{t-r/\beta}$	R^{-1}	$r^{-3/2}$
intermediate field	$\delta(t-R/c)$	$1/\sqrt{t-r/c}$	R^{-1}	$r^{-1/2}$
far field	$\frac{\partial}{\partial t}\delta(t-R/c)$	$\frac{\partial}{\partial t}(1/\sqrt{t-r/c})$	R^{-1}	$r^{-1/2}$

As shown in Table 1, their amplitudes differ by a factor $r^{-1/2}$ of in all terms, and a tail exists in the waveform due to line sources. Note that $\sqrt{t-r/c}$ is the integration of $1/\sqrt{t-r/c}$. By means of the exchangeability between convolution and derivation, one can obtain

$$\left.\begin{aligned}
&\frac{1}{\sqrt{t}} * \sqrt{t-r/c} = \frac{\pi}{2} H(t-r/c)(t-r/c),\\
&\frac{1}{\sqrt{t}} * \frac{1}{\sqrt{t-r/c}} = \pi H(t-r/c),\\
&\frac{1}{\sqrt{t}} * \frac{\partial}{\partial t}\frac{1}{\sqrt{t-r/c}} = \pi\delta(t-r/c).
\end{aligned}\right\} \tag{15}$$

where * means convolution. Applying the operator $\frac{\partial}{\partial t}\frac{1}{\sqrt{t}}*$ to the linear source response, we obtain

$$\begin{aligned}
&C\frac{\partial}{\partial t}\frac{1}{\sqrt{t}} * u_i^L\\
&-\frac{C}{2\pi\rho}\left(\frac{8\gamma_i\gamma_j\gamma_k-2\gamma_i\delta_{jk}-2\gamma_j\delta_{ik}-2\gamma_k\delta_{ij}}{r^{3/2}}\right)\frac{\pi}{\sqrt{2}}\left[\frac{1}{\sqrt{\alpha}}H(t-r/\alpha)-\frac{1}{\sqrt{\beta}}H(t-r/\beta)\right]m_{jk}\\
&+\frac{C}{2\pi\rho\alpha^2}\left(\frac{4\gamma_i\gamma_j\gamma_k-\gamma_i\delta_{jk}-\gamma_j\delta_{ik}-\gamma_k\delta_{ij}}{r^{3/2}}\right)\frac{\pi}{\sqrt{2}}\sqrt{\alpha}\,\delta(t-r/\alpha)m_{jk}\\
&-\frac{C}{2\pi\rho\beta^2}\left(\frac{4\gamma_i\gamma_j\gamma_k-\gamma_i\delta_{jk}-\gamma_j\delta_{ik}-2\gamma_k\delta_{ij}}{r^{3/2}}\right)\frac{\pi}{\sqrt{2}}\sqrt{\beta}\,\delta(t-r/\beta)m_{jk}\\
&+\frac{C}{2\pi\rho\alpha^3}\gamma_i\gamma_j\gamma_k\frac{1}{r^{1/2}}\frac{\pi}{\sqrt{2}}\sqrt{\alpha}\frac{\partial}{\partial t}\delta(t-r/\alpha)m_{jk}\\
&\qquad-\frac{1}{2\pi\rho\beta^3}(\gamma_i\gamma_j-\delta_{ij})\gamma_k\frac{1}{r^{1/2}}\frac{\pi}{\sqrt{2}}\sqrt{\beta}\frac{\partial}{\partial t}\delta(t-r/\beta)M_{jk}.
\end{aligned} \tag{16}$$

After the above transforms the waveforms in equation (16) become similar to that of the point source response. To further correct the geometrical spreading factor, a factor C is introduced in (16). Comparing the terms in equation (16) with the corresponding terms in (13), it can be seen that for waves propagating with the compressional velocity a factor $C = C_0/(\pi\sqrt{2r\alpha})$ is needed whereas for waves propagating with the transverse velocity we need a factor $C = C_0/(\pi\sqrt{2r\beta}$, where $C_0 = M_0/m_0$, r is the distance the wave propagated. Generally r is easily determined for direct waves, but for multi-reflected waves, to determine their travel distances is very difficult. As an approximation we use the travel time to evaluate the travel distance. When $t \le t_\beta$, the main phases are various direct waves. The source-receiver r_0 distance is used in the correction. For direct compressional waves

$$C = \frac{C_0}{\pi}\frac{1}{\sqrt{2r\alpha}} = \frac{C_0}{\sqrt{2}\,\pi}\frac{\sqrt{t_\alpha}}{r_0},$$

and for direct transverse waves

$$C = \frac{C_0}{\pi}\frac{1}{\sqrt{2r\beta}} = \frac{C_0}{\sqrt{2}\,\pi}\frac{\sqrt{t_\beta}}{r_0}.$$

in which t_α and t_β are the travel times of compressional and transverse waves respectively. When $t > t_\beta$, compressional waves are relatively weak and the travel time of transverse waves is used for the correction.

$$C = \frac{C_0}{\pi}\frac{1}{\sqrt{2r\beta}} = \frac{C_0}{\sqrt{2}\,\pi}\frac{1}{\bar{\beta}}\frac{1}{\sqrt{t}}.$$

where $\bar{\beta}$ is the average transverse velocity along the path. In conclusion, the correction operator for obtaining a point source response is

$$C(t) \cdot \frac{\partial}{\partial t}\frac{1}{\sqrt{t}} * , \tag{17}$$

in which

$$C(t) = \begin{cases} \dfrac{C_0}{\sqrt{2}\,\pi}\dfrac{\sqrt{t}}{r_0}, & t \leqslant t_\beta; \\ \dfrac{C_0}{\sqrt{2}\,\pi}\dfrac{1}{\bar{\beta}}\dfrac{1}{\sqrt{t}}, & t > t_\beta. \end{cases} \tag{18}$$

Now we will give a brief discussion about the accuracy and errors of the approximate point source response. First, the waveforms and the powers in the geometrical spreading factors for all the near-field, intermediate-field, and far-field terms are basically accurate. The amplitudes and radiation patterns of the far-field terms are nearly accurate. In the intermediate field, the term with $\gamma_i \gamma_j \gamma_k$ is 1/3 smaller than the corresponding point source term. The amplitudes of the near-field term is 1/3-1/2 smaller than that of the corresponding point source term. For seismic sources, the near-field terms are mainly composed of broad pulse and static deformations; therefore, the errors mentioned above will not seriously affect the high frequency seismograms. On the other hand, when we evaluate the travel distance with the average velocity $\bar{\beta}$, the amplitudes of reflected compressional waves, which may arrive at the receiver later than the direct transverse waves, may be over-estimated, and also the value of the average velocity $\bar{\beta}$ will slightly affects the results. Because the corrections to the original geometrical spreading factors have a form of $r^{-1/2}$, they will not seriously affect the results. In the point source solutions for a strike-slip fault or an explosive source, there are contributions from the moment tensor component M_{22}, but they are lacking in two-dimensional problems. It can be shown that this will only affect the radial component of near-field vibrations in the x_1ox_3 plane, so we shall not make further compensations for them. The approximation errors mentioned above will be further discussed in section V by comparing with the more accurate solutions.

IV. FINITE-DIFFERENCE METHOD

Generally the finite-difference schemes can be divided into "homogeneous formulation" and "heterogeneous formulation" (Kelley et al., 1976). The former deals with the

boundaries between the different media explicitly, and in the latter the media properties may be specified at each grid point of a finite-difference mesh, while the interface conditions are satisfied automatically. The finite-difference scheme used in the present research is a generalization of the MacCormack-type multistep method developed by Gotllieb and Turkel (1976). This is a heterogeneous scheme with the fourth-order accuracy in space and second-order accuracy in time, and has been successfully used to solve the propagation problems of elastic waves (Bayliss et al., 1986). Because the fourth-order scheme has higher accuracy and lower grid dispersion, this method allows to obtain the required accuracy with a relatively coarse grid.

The standard first-order partial differential system in one dimension can be written as

$$\frac{\partial U}{\partial t} = \frac{\partial f}{\partial x} + h, \tag{19}$$

The present finite-difference scheme divided the calculation from one time step into two steps, the formulas are

$$U_n^{(1)} = U_n^k + \frac{\lambda}{6}\left(-f_{n+2}^k + 8f_{n+1}^k - 7f_n^k\right) + \Delta t h_n^k,$$

$$U_n^{k+1} = \frac{1}{2}\left(U_n^k + U_n^{(1)}\right) + \frac{\lambda}{12}\left(7f_n^{(1)} - 8f_{n-1}^{(1)} + f_{n-2}^{(1)}\right) + \frac{\Delta t}{2} h_n^{(1)}. \tag{20}$$

where U is the vector of unknowns, f and h are vector functions of U, x and t, $\lambda = \Delta t/\Delta x$, the subscript n denotes the spatial grid point and the superscript k denotes the time level, $f^{(1)} = f(U^{(1)})$, $h^{(1)} = h(U^{(1)})$, terms with superscript (1) denote the intermediate values. The method first obtained an intermediate value $U^{(1)}$ at each point using forward differences to approximate the spatial derivatives. The intermediate value is then used in the second equation, using the backward differences, to obtain the values U^{k+1}. There is a revision of equation (20), which first used the backward difference and then the forward difference. Equation (20) is known to be stable, provided that $\alpha(\Delta t / \Delta x) \leq 0.67$. It is possible to extend the above scheme directly to two dimensions, but complicated mixed derivatives will be present. Instead of doing this we shall adopt another algorithm, which is based on the dimensional splitting technique, i.e., to update the two-dimensional problems for one time step, the one- dimensional formula is repeatedly used twice, once in x_1 direction and once in x_3 direction. The finite-difference code for this method is very simple and suitable for vector computers.

In the basic equation (4), A and B are composed of the media parameters, which depend on the spatial coordinate, so it is not an equation of the standard form. By means of linear manipulations (Bayliss, et al. 1986), equation (4) can be rewritten as

$$E_0 \frac{\partial w}{\partial t} = A_0 \frac{\partial w}{\partial x_1} + B_0 \frac{\partial w}{\partial x_3} + E_0 s_{P-SV}. \tag{21}$$

in which

$$\mathbf{E}_0 = \begin{bmatrix} \rho & 0 & 0 & 0 & 0 \\ 0 & \rho & 0 & 0 & 0 \\ 0 & 0 & \dfrac{\lambda+2\mu}{(\lambda+2\mu)^2-\mu^2} & \dfrac{-\mu}{(\lambda+2\mu)^2-\mu^2} & 0 \\ 0 & 0 & \dfrac{-\mu}{(\lambda+2\mu)^2-\mu^2} & \dfrac{\lambda+2\mu}{(\lambda+2\mu)^2-\mu^2} & 0 \\ 0 & 0 & 0 & 0 & \dfrac{1}{\mu} \end{bmatrix}, \tag{22}$$

$$\mathbf{A}_0 = \begin{bmatrix} 0 & 0 & 1 & 0 & 0 \\ 0 & 0 & 0 & 0 & 1 \\ 1 & 0 & 0 & 0 & 0 \\ 0 & 0 & 0 & 0 & 0 \\ 0 & 1 & 0 & 0 & 0 \end{bmatrix}, \quad \mathbf{B}_0 = \begin{bmatrix} 0 & 0 & 0 & 0 & 1 \\ 0 & 0 & 0 & 1 & 0 \\ 0 & 0 & 0 & 0 & 0 \\ 0 & 1 & 0 & 0 & 0 \\ 1 & 0 & 0 & 0 & 0 \end{bmatrix}. \tag{23}$$

Here E_0 is independent of t, A_0 and B_0 are independent of x_1 and x_3. Let $U = E_0 w$, $f = A_0 w = A_0 E_0^{-1} U$, $g = B_0 w = B_0 E_0^{-1} U$, $h = E_0 s_{P-SV}$. A comparison with equation (19) shows that equation (21) has the standard form. Since equation (21) is obtained from equation (4) by linear manipulations, the same algorithm can also be used to solve equation (4).

In seismology, we usually deal with the wave propagation problems in infinite or semi-infinite media. But the finite-difference calculations have to be carried out in a finite domain. To choose the appropriate boundary conditions and avoid their effects on the wave field is an important issue. For this purpose, some sorts of artificial boundary conditions, known as absorbing or transmitting boundaries, are needed, for example the paraxial boundary by Clayton and Engquist (1977, 1980), the viscous boundary by Lysmer and Kuhlemeyer (1969), and the transmitting boundary by Liao et al. (1984), and etc. The first-order paraxial boundary and viscous boundary are adopted by most of the authors for their simplicities. The boundary conditions developed by Bayliss et al. (1986), which has been shown to be stable on the free surface and equivalent to the first-order paraxial boundary or viscous boundary on the artificial boundaries, are used in our calculation.

The grid sizes in space and time are closely related to the stability and numerical dispersion. These factors should be analyzed jointly (Alford et al., 1974, Baylies et al., 1986) and determined with the assist of numerical experiments.

Table 2

Media parameters for the elastic half-space model

h (km)	α (km/s)	β (km/s)	ρ (g/cm^3)
∞	6.20	3.50	2.70

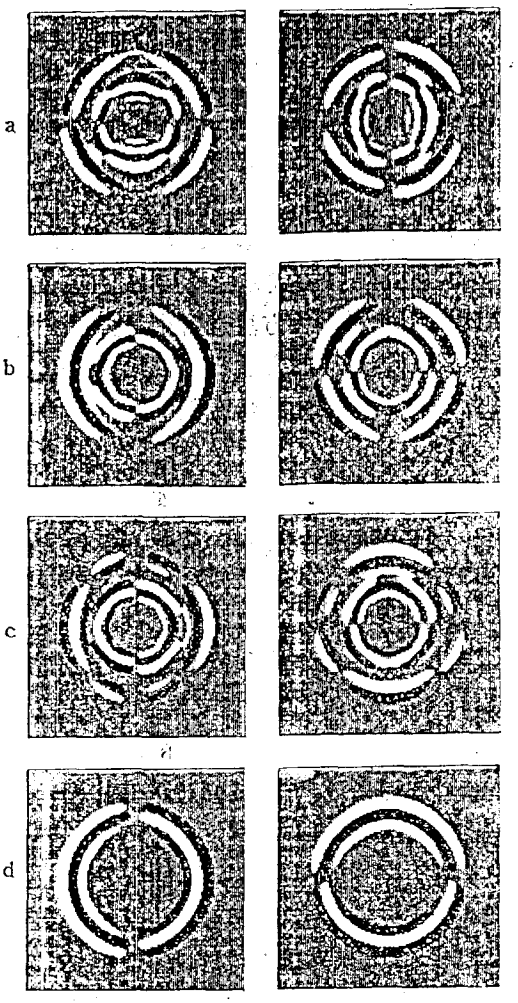

Fig. 2.
Wave fields produced by various sources.
(a) dip-slip fault. (b) strike-slip fault. (c) 45° dip-slip fault (d) explosive source. The horizontal component is shown on the left and the vertical component is shown on the right.

Table 3
Media parameters for the model of one layer over a half-space

h (km)	α (km/s)	β (km/s)	ρ (g/cm^3)
5.0	3.50	2.00	2.40
∞	5.50	2.30	2.70

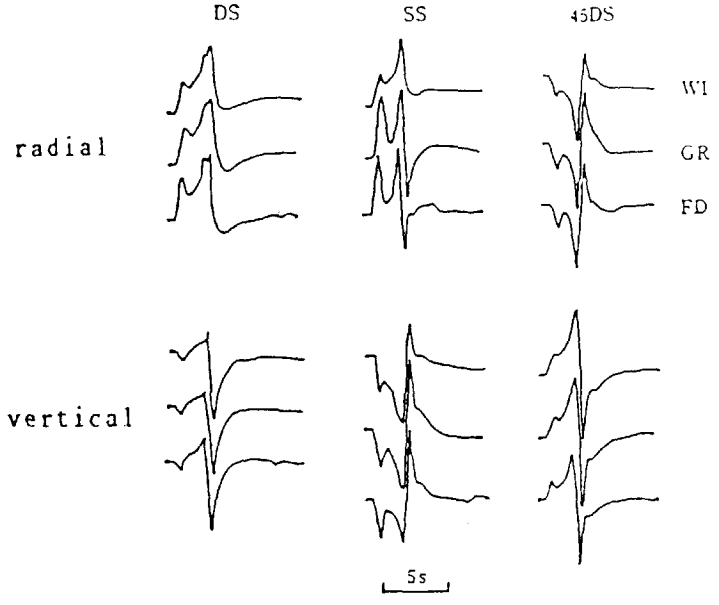

Fig. 3.

Comparison of the radial and vertical displacements due to three fundamental faults in a half-space. The result from wavenumber integration method is denoted with WI; the result from generalized ray theory is denoted with GR and the result from finite-difference method proposed by the authors is denoted with FD. The focal depth is 8km, the receiver is on the free surface with an epicenter distance of 16km and the parameters of the half-space model are listed in Table 2.

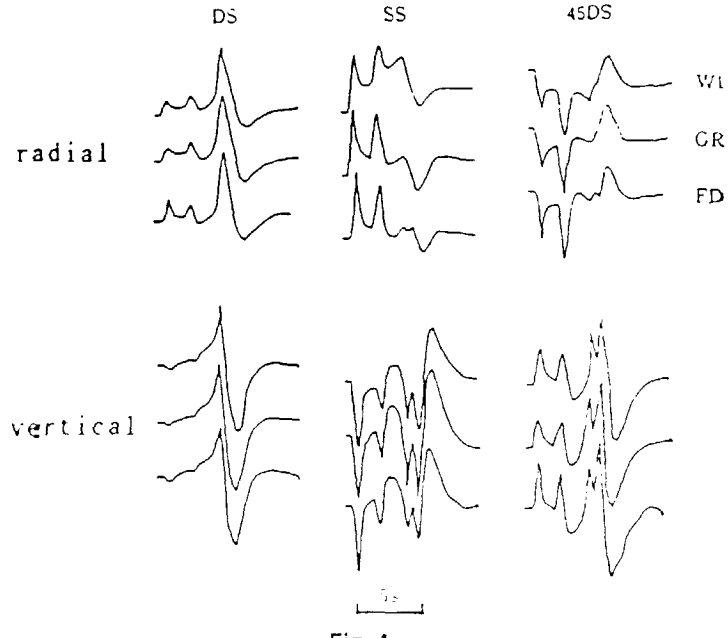

Fig. 4.

Same as Figure 3, except that the epicenter distance is 32km.

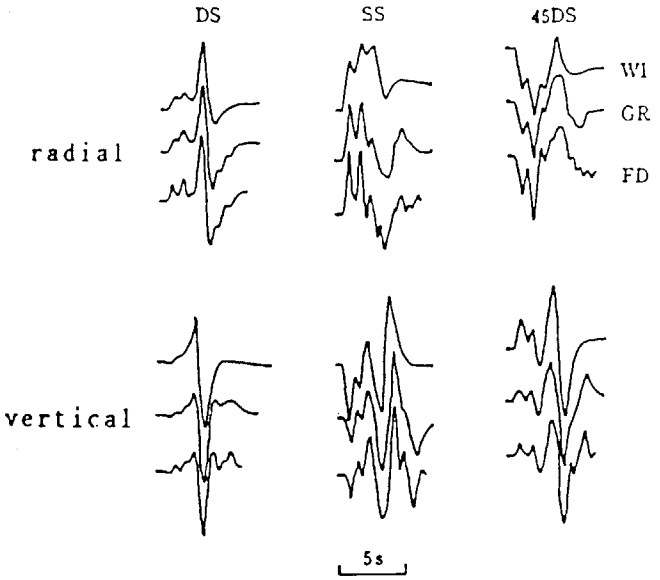

Fig. 5.

Comparison of the radial and vertical displacements due to three fundamental faults in one layer over a half-space model. The result from wavenumber integration method is denoted with WI; the result from generalized ray theory is denoted with GR and the result from finite-difference method proposed by the authors is denoted with FD. The focal depth is 2.5km, the receiver is on the free surface with an epicenter distance of 10km, and the parameters of the one layer over a half-space model are listed in Table 3.

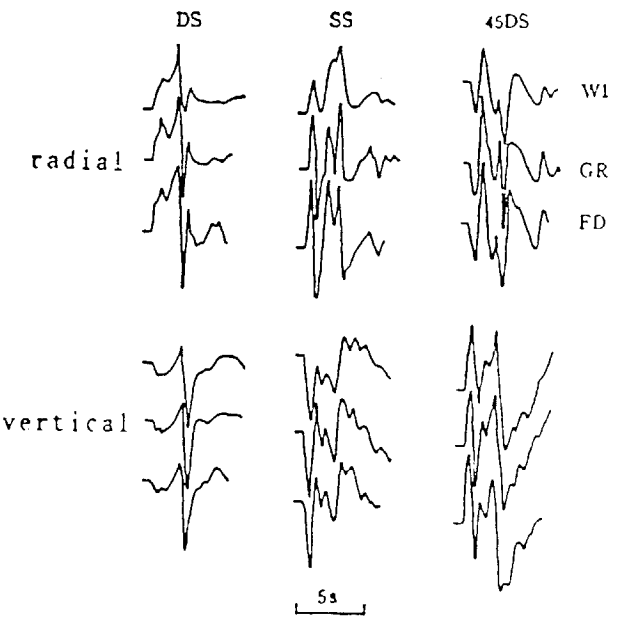

Fig. 6.

Same as Figure 5, except that the source is below the top layer at a depth of 7km.

V. NUMERICAL RESULTS AND DISCUSSION

Figure 2 shows the time slices of the wave field for the dip-slip, strike-slip, and 45° dip-slip faults as well as the explosive source. For dislocation sources, we can see clearly that the outer rings are faster compressional waves and the inner rings are slower transverse waves. The familiar radiation patterns and nodal planes for both waves are also clear. For explosive source, there are only compressional waves.

To examine the reliability and applicability of the numerical scheme, the responses of an elastic half-space or layered half-space model are calculated and compared with the more accurate solutions. As a first numerical example, we calculate the radial and vertical displacements at the free surface due to the three fundamental types of faults in an elastic half-space, for which the media parameters are listed in Table 2. The synthetic seismograms are shown in Figures 3 and 4. The far-field source time history is a Gaussian pulse with a width of about one second, the focal depth is 8km and the epicenter distances are 16km (Figure 3) and 32km (Figure 4), respectively. For comparison, the results from two other methods are also shown in these figures, in which the broad band wavenumber integration solution is denoted with WI and the high frequency approximation of generalized ray solution is denoted with GR, the finite-difference approximation proposed by the present research is denoted with FD. The responses for models of one layer over a half-space are shown in Figures 5 and 6, the media parameters are listed in Table 3. The source time history is the same as that used in the previous calculations, and the epicenter distance is 10km. For Figure 5 the source is in the top layer at a depth of 2.5km, and for Figure 6 the source is below the top layer at a depth of 7.0km. For comparison the amplitudes from the above calculations are listed in Table 4.

Table 4

The comparisons between the amplitudes from various methods

fault type	depth (km)	epi-center (km)	radial			vertical		
			WI	FD	GR	WI	FD	GR
DS	8.0	16.0	7.0	4.2	4.8	8.1	7.3	7.9
SS	8.0	16.0	6.4	3.0	2.0	3.1	2.6	1.0
45DS	8.0	16.0	6.8	5.6	4.1	4.4	5.1	4.4
DS	8.0	32.0	3.2	2.6	2.8	3.2	2.7	3.2
SS	8.0	32.0	1.9	1.5	1.3	0.6	0.6	0.5
45DS	8.0	32.0	2.5	2.3	1.9	1.1	0.9	1.0
DS	2.5	10.0	89.7	80.1	73.2	101.3	110.8	110.6
SS	2.5	10.0	54.8	35.4	34.7	14.8	31.2	26.9
45DS	2.5	10.0	65.7	68.5	64.9	29.3	71.2	63.9
DS	7.0	10.0	29.0	16.9	25.8	28.0	26.6	42.4
SS	7.0	10.0	19.7	7.9	11.4	9.3	8.4	10.1
45DS	7.0	10.0	18.1	14.9	19.4	9.6	9.8	13.8

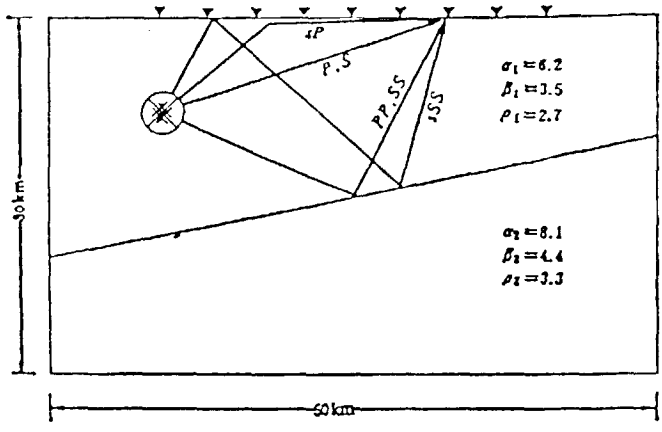

Fig. 7.

The geometry of the structure, source and receiver used to show the effect of an inclined interface, along with the parameters of the media and the main phases.

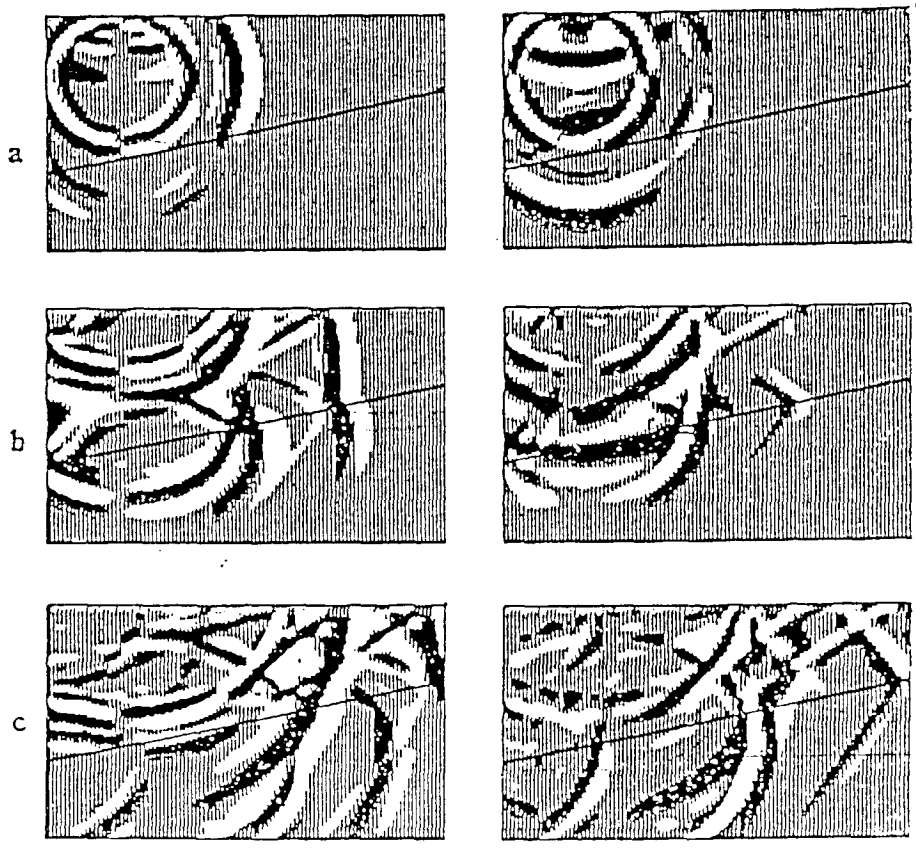

Fig. 8.

Wave field in the media shown in Figure 7. The horizontal component is shown on the left and the vertical component is shown on the right.

(a) t = 3s.

(b) t = 5s.

(c) t = 7s.

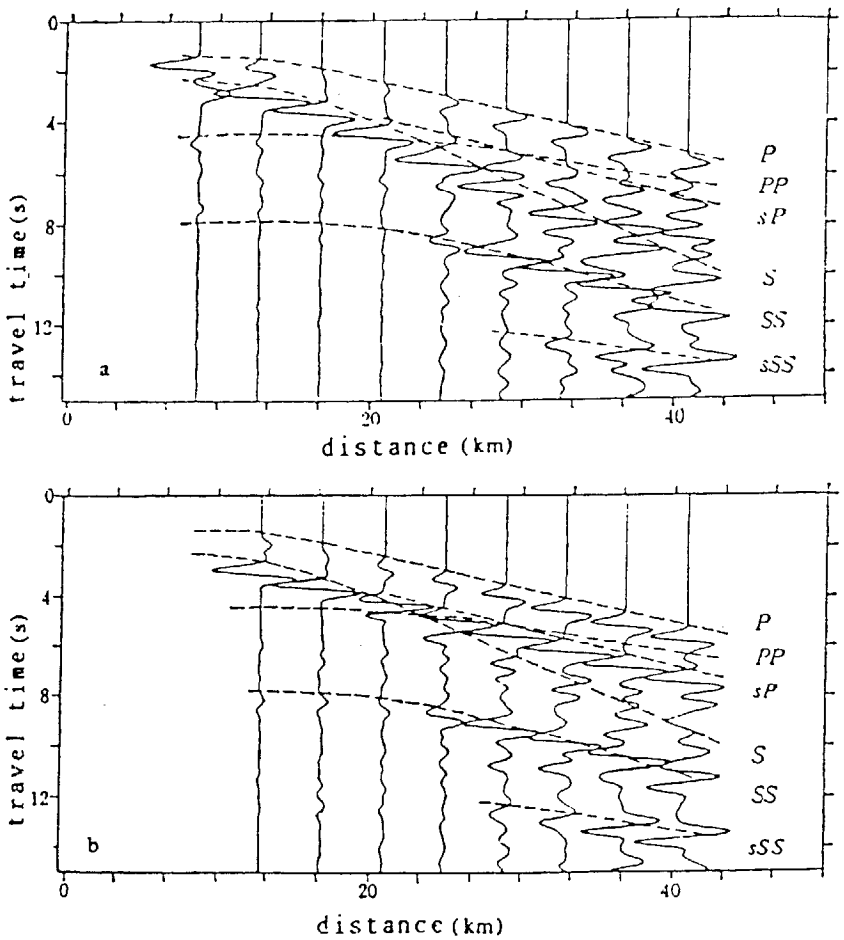

Fig. 9.
Synthetic seismograms for the model shown in Figure 7, along with the travel time curves for various phases. (a) vertical component, (b) horizontal component.

In Figures 3 to 6, the results from the three methods show good agreement. Careful analyses show that there are more low frequency contents in the accurate wavenumber integration solutions but they are lacking in the high frequency approximation of the generalized ray solution. The finite-difference solution is relatively closer to the high frequency approximation of generalized ray solution. These discrepancies come at first from the fact that some quantities in the near-field term of our approximate solution are smaller than the corresponding terms for the point source. In addition, the low frequency contents are partly suppressed by correction operator (17). These discrepancies can also be noticed in Table 4, in which most of the amplitudes of finite-difference solutions lie between the accurate solutions and those of the high frequency approximations. In conclusion, the accuracy of the finite-difference solution is a little higher than that of the high frequency approximation. Compared with the accurate wavenumber integration solution, the errors are mainly in the low frequency contents and static responses.

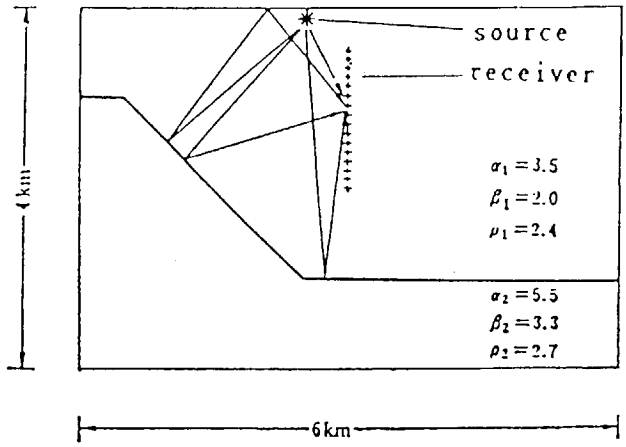

Fig. 10.
The geometry of the structure, source and receivers used in VSP simulation in a simple uplift structure.

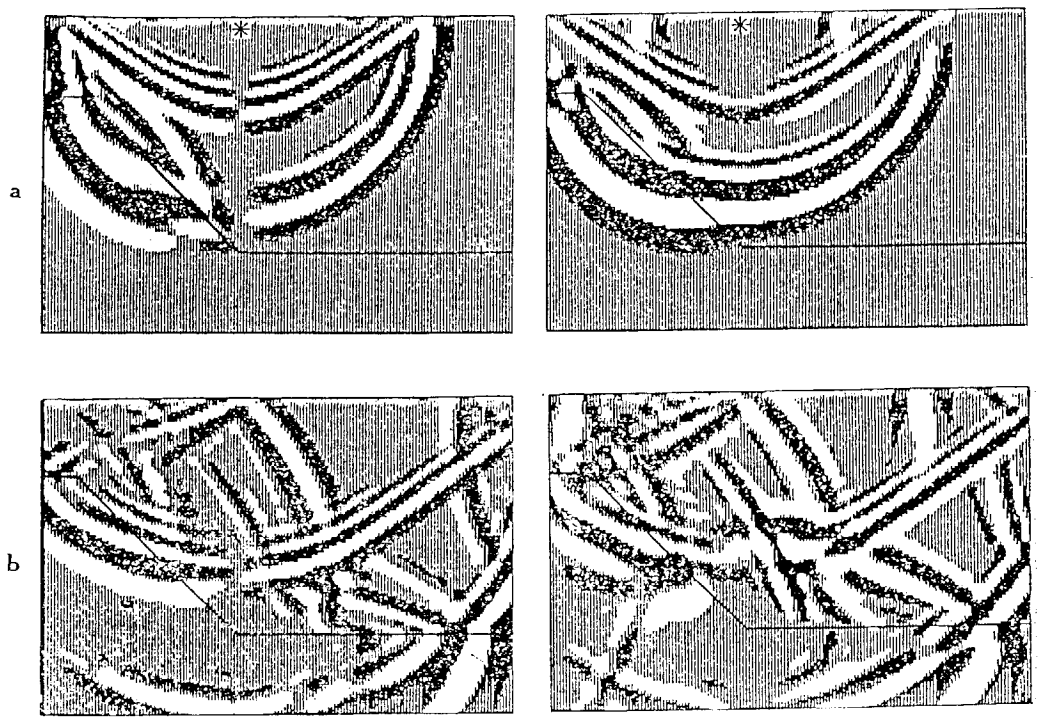

Fig. 11.
Wave field in the media, whose structure is shown in Fig. 10. The horizontal component is shown on the left and the vertical component is shown on the right; "*"depicts the position of the source. (a) t=1.0s. (b) t=1.5s.

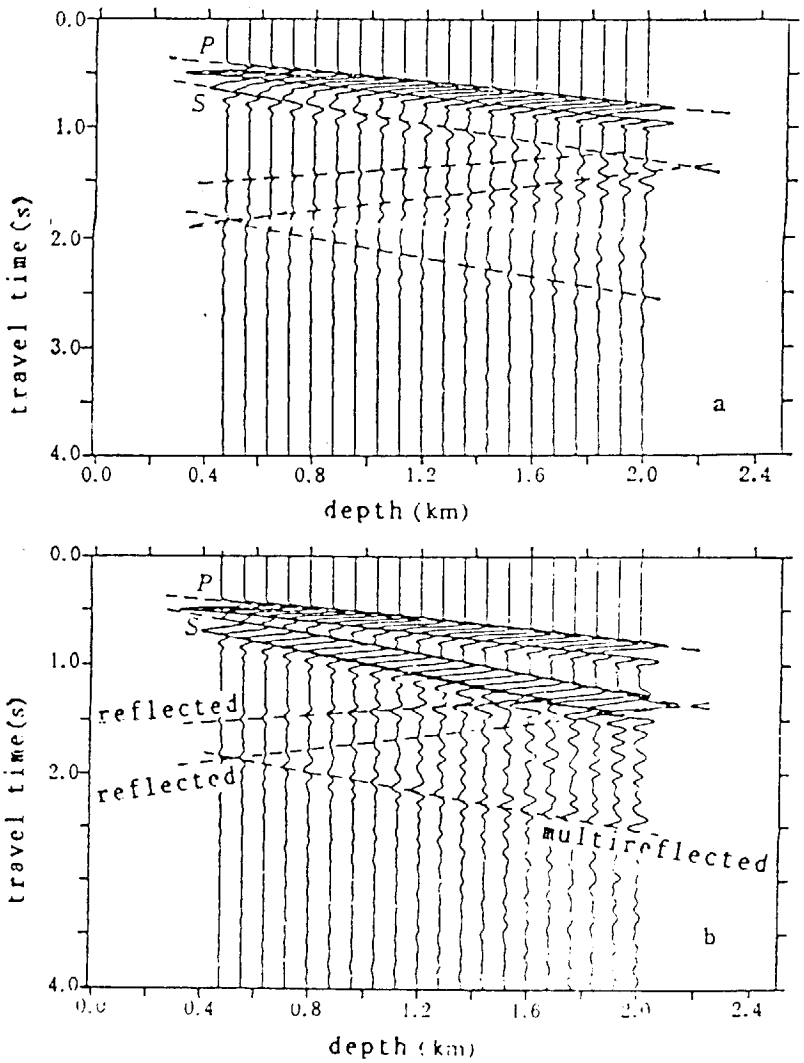

Fig. 12.

Synthetic seismograms in VSP simulation. The structure is shown in Figure 10. (a)vertical component. (b) horizontal component.

The most important advantage of the finite-difference methods is their applicability to wave propagation problems in complicated structures. Two numerical examples with complex interfaces are given here. In Figures 7 to 9, the response from a 45 dip-slip fault buried in a half-space with an inclined interface is shown. Figure 7 shows the geometry of the media, source and receiver, as well as the media parameters and the main phases. Figure 6 shows the timeslices of the wave fields, the horizontal component is shown on the left and the vertical component on the right. In timeslices at t = 3s, direct P-wave, S-wave and their reflections from the free surface can be clearly distinguished. Note that

the *P*- and *S*-waves show different appearances in the horizontal and vertical components owing to their different polarizations. In timeslices at $t = 5$s, we can see the waves reflected and refracted at the inclined interface. On the right, near the interface we can see the formation of the head wave. In timeslices at $t = 7$s, the wave fields become quite complicated, on the right we can see the head wavefront clearly. Figure 9 shows the synthetic seismograms and travel time curves for various phases. Near a distance of 17km, there is the *P*-wave nodal plane. In the vicinity of it the amplitude of the *P*-wave is very small, and the sign of the first motion is opposite across the nodal plane.

Figures 10 to 12 show a VSP simulation for a simple uplift structure. Figure 10 gives the structure and the positions of the explosive source and the receivers, The interface is composed of an inclined segment and a horizontal segment. Figure 11 shows the interaction between a shallow explosive source and the complicated interface. In the wave field at $t = 1.0$s, since the source depth is very shallow the direct *P*-wave and *pP* phases reflected from the free surface are superposed and propagated downward, followed by the *pS* phase reflected from the free surface. Between the wave front of the *pS* phase and the free surface, on both sides of the source, there is the Rayleigh wave. The left wing of the *P*-wave has arrived at the inclined segment of the interface and produced the reflected and refracted phases, but the time is too short to separate the compressional and transverse waves in these phases. In the wave field at $t = 1.5$s, the direct *P*-wave has arrived at the horizontal segment of the interface, meanwhile the downward *pS* phase has arrived at the inclined interface and produced the reflected and refracted waves, respectively. In addition, the reflected waves, which are produced by the direct P-wave on the inclined segment, have propagated a considerable distance, and the compressional and transverse phases have been clearly separated, the reflected *P*-waves from the inclined interface is again reflected downward by the free surface as compressional and transverse waves. Figure 12 illustrates the synthetic seismograms for the VSP experiment.

In conclusion, we have presented a finite-difference method to calculate the *P-SV* wave responses for a point source in two-dimensional heterogeneous media (inside the incident plane). Since there are no effective methods for calculating the point source responses in laterally varying media, we first derived the correction operator analytically for homogeneous media, then examined the accuracy of the approximate solutions by comparing it with the accurate result in vertically heterogeneous media. Since the finite-difference code and the correction operator for waveform and amplitude is independent of the specific structure, the present approximate method is suitable for computing the responses due to point dislocation source, explosive source, or concentrated body force in laterally heterogeneous media, which is very important in research of problems such as the near source strong ground motion, explosive vibration or seismic exploration. To extend the present method to *SH*-wave is straightforward which will be presented in our following papers.

ACKNOWLEDGEMENT

The authors wish to thank Professor C. Y. Fu for his continued encouragements throughout the present research.

REFERENCES

[1] Aki, K.and Richards, P. G., Quantitative Seismology Theory and Methods, W. H., Greeman and Company, San Francisco, 1980.
[2] Alford, R.M., Kelly, K. R. and Boore, D. M., Accuracy of finite-difference modelling of the acoustic wave equation, *Geophysics*, 39, 834-842, 1974.
[3] Alterman, A. and Karal, F. C., Propagation of elastic waves in layered media by finite difference methods, *Bull. Seism. Soc. Am.*, 58, 367-398.
[4] Bayliss, A., Jordan, K. E., Lemesurier, B. J. and Turkel, E. A fourth-order accurate finite-difference scheme for the computation of elastic waves, *Bull. Seism. Soc. Am.*, 76, 1115- 1132, 1986.
[5] Bouchon, M., Discrete wavenumber representation of elastic wave fields in three dimensions, *J. Geophys. Res.*, 84, 3609-3614, 1979.
[6] Clayton, R. W. and Engquist, B., Absorbing boundary conditions for acoustic and elastic wave equations, *Bull. Seism. Soc. Am.*, 67, 1529-1540, 1977.
[7] Clayton, R. W. and Engquist, B., Absorbing boundary conditions for wave-equation migration, *Geophysics*, 45, 895-904, 1980.
[8] Gottlieb, D. and Turkel, E., Dissipative two-four methods for time-dependent problems, *Math. Comp.*, 30, 703-723, 1976.
[9] Helmberger, D. V., The crust-mantle transition in the Bering Sea, *Bull. Seism. Soc. Am.*, 58, 179-214, 1968.
[10] Kelly, K. R., Ward, R. W., Treitel, S. and Alford, R. M., Synthetic seismograms: a finite difference approach, *Geophysics*, 41, 2-27, 1976.
[11] Li You-ming, An algorithm in term of dissolved Haskell- matrices for near-field synthetic seismograms, *Earthq. Res. China* (in Chinese), 1, 2, 36-44, 1985.
[12] Liao Zhen-peng, Wong, H. L., Yang Bai-po and Yuan Yi-fan, A transmitting boundary for transient wave analyses, *Scientia Sinica* (Series A), 17, 1063-1076, 1984.
[13] Lysmer, J. and Kuhlemeyer, R. L., Finite dynamic model for infinite media, J. Eng. Mechanics Div. Asce, 859-877, 1969.
[14] Olson, A. H., Orcutt J. A. and Frazier, G. A., The discrete wavenumber/finite element method for synthetic seismograms, *Geophys. J. Roy astr. Soc.*, 77, 421-460, 1984.
[15] Vidale, J. E., Application of two-dimensional finite difference wave simulation to earthquake, earth structure and seismic hazard, PhD. thesis, California Institute of Technology, Pasadena, California, 1987.
[16] Vidale, J. E., Helmberger, D. V. and Clayton, R. W., Finite difference seismograms for SH waves, *Bull. Seism. Soc. Am.*, 75, 1765-1782, 1985.
[17] Virieux, J., SH-wave propagation in heterogeneous media: Velocity-stress finite-difference method, *Geophysics*, 49, 1933- 1957, 1984.
[18] Virieux, J., P-SV wave propagation in heterogeneous media: Velocity-stress finite-difference method, *Geophysics*, 51, 889- 901, 1986.

[19] Yao, Z. X. and Harkrider,D. G., A Generalized reflection- transmission coefficient matrix and discrete wavenumber method for synthetic seismograms, *Bull. Seism. Soc. Am.*, 73, 1685-1699, 1983.

[20] Yuan, Y., Yoshizawa, S. and Osawa, Y., Strong ground motion simulation of the 1976 Ninghe, China earthquake, *Bull. Earthq. Res. Inst. Univ. Tokyo*, 61, 97-127, 1986.